Conformations of 1,1-Dimethoxyethane: Matrix Isolation Infrared and ab Initio Studies

V. Venkatesan, K. Sundararajan, and K. S. Viswanathan*

Materials Chemistry Division, Indira Gandhi Centre for Atomic Research, Kalpakkam 603 102, India

Received: March 20, 2002; In Final Form: June 17, 2002

Conformations of 1,1-dimethoxyethane (DME) were studied using matrix isolation infrared spectroscopy. DME was trapped in an argon matrix using an effusive source maintained at temperatures over the range 298−431 K. Deposition was also done using a supersonic jet source to look for conformational cooling in the expansion process. As a result of these experiments, infrared spectra of the ground and first higher-energy conformer of DME are reported for the first time. The experimental studies were supported by ab initio computations performed at HF and B3LYP levels, using a 6-31++G** basis set. Computationally, five minima were identified corresponding to conformers with **G**$^-$**G**$^+$, **TG**$^-$, **TG**$^+$, **TT**, and **G**$^+$**G**$^+$ structures, given in order of increasing energy. The computed frequencies at the B3LYP level for the **G**$^-$**G**$^+$ and **TG**$^-$ conformers were found to compare well with the experimental matrix isolation frequencies, leading to a definitive assignment of the infrared features of DME for these conformers. At the B3LYP/6-31++G** level, the energy difference between the **G**$^-$**G**$^+$ and **TG**$^-$ conformers was computed to be 0.67 kcal/mol.

Introduction

It has been known for a long time that competition between anomeric and steric interactions plays an important role in determining the conformational stabilities of simple acetals, such as dimethoxymethane (DMM). In DMM, for example, the anomeric interactions, where nonbonded electron density orients itself antiperiplanar to an adjacent C−O bond, dominate to direct each of the C−O−C−O and O−C−O−C groups to adopt a gauche orientation, which maximizes the n−σ* interaction. The GG conformer consequently is the ground-state conformer, followed by structures in which the anomeric interactions are progressively decreased to form conformers which have the C−O−C−O groups with a trans orientation, i.e., the TG and TT conformers. It may be recalled that the TT form which is the least stable in DMM is the equivalent of the most stable structure in *n*-pentane. This situation arises because unlike in DMM, there are no anomeric interactions in the hydrocarbons that can counterbalance the gauche steric interactions, leading therefore to TT structures as the most stable in hydrocarbons. The physical evidence for the GG conformation in acetals and ketals is described in detail in many texts on stereoelectronic effects.[1−3] Calculations also support the above observations.[4−6] Recently, we published a detailed experimental and computational study on the conformers of DMM, wherein we had presented infrared spectra for the ground state, GG, and the first higher-energy, TG, conformers of DMM isolated in solid Ar matrixes.[7] These experiments were done using supersonic as well as hot nozzle effusive sources to deposit the matrix.

In acetals $R^1CH(OR^2)OR^3$, when the central atom substituent $R^1 \neq H$, we have gauche steric interactions along the central C−O bonds. Likewise, the steric interactions of the terminal substituents R^2 or R^3 are also possible in such acetals. Consequently, the conformation problem in such compounds can become quite complex. 1,1-Dimethoxyethane (DME) is the first of this series of compounds and, thus, serves as a good model compound for the study of the interplay of anomeric and steric effect in acetals.

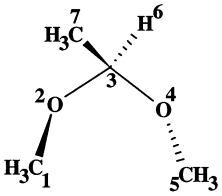

Figure 1. Structure of DME to show the atom numbering.

There has been some ambiguity in the literature regarding the notation adopted to denote the conformers of acetals. It may therefore not be out of place to first describe our notation to denote the conformers before we proceed to discuss the conformers of DME.

The various conformers arise from the different orientation of the terminal carbon atoms (C1 and C5) with respect to the plane defined by O2−C3−O4 atoms (Figure 1). If C1 is oriented gauche with respect to O4, it is denoted by G and, if oriented trans, by T. Similarly, the orientation of C5 with respect to O2 is denoted by G or T. Furthermore, if both C1 and C5 are oriented on the same side of the O2−C3−O4 plane, they are denoted by the same superscript sign, i.e., G^+G^+ or G^-G^-; if they are oriented on opposite sides of the reference plane, they are denoted by G^+G^- or G^-G^+. In the case of DMM, the symmetry of the molecule renders both sides of the reference plane equivalent; however, in the case of DME, the presence of a methyl group on the central carbon atom (C3) renders the two sides of the reference plane nonequivalent. The side on which the methyl group on C3 is located is denoted by + superscript (G^+), while the side where a hydrogen on C3 is located is denoted by a − sign (G^-). This notation therefore implies, for example, that the conformer G^+G^+ has both terminal methyl groups and the methyl on C3 on the same side of the reference plane.

This notation is slightly at variance with that used in our earlier work on DMM. We had in that work denoted the ground-

* Corresponding author. E-mail: vish@igcar.ernet.in.

10.1021/jp025793l CCC: $22.00
Published on Web 07/26/2002

state conformer of DMM as GG, while using the present notation, the same conformer should be designated as G^+G^- (which of course is degenerate with G^-G^+). In the same work, we had also identified a conformer located ~3.6 kcal/mol above the ground-state conformer and had denoted it as G^+G^-. However, in the present notation, the same conformer should be designated as G^+G^+ (or the equivalent G^-G^-). The other conformer of DMM, TG, would have two degenerate forms, TG^- and TG^+. We believe that this notation helps to easily identify the relative location of the terminal methyl groups and has therefore been adopted. When discussing structures quoted in the literature, we have reproduced the notation used in the respective papers, but alongside each of those representations, we have also given in parentheses and in bold font the corresponding representation in our notation. Henceforth in this paper, all structures denoted are consistent with our notation have been shown in boldface font.

DME. The first studies on the structure of DME date back to 1968, where Goodman and Niu[8] suggested from dipole moment studies and classical potential function calculations that a TG conformer was the most stable. However, an infrared study on DMM by Saur et al.[9] concluded that the most stable conformer of DME was a GG form. In addition, they also saw some evidence for higher-energy conformers of DME in their experiment. However, the experimental data was sparse for any definitive assignment to be made for the higher-energy conformers of DME. Furthermore, in the liquid and solid phase, the infrared spectral features of the different conformers were not resolved, and unambiguous assignments were therefore not possible. Measurements using ^{17}O NMR[10] indicated that a G^+G^+ or the equivalent G^-G^- (**G**$^+$**G**$^-$ or **G**$^-$**G**$^+$ in our notation) structure was the most stable. A later work using ^{13}C NMR[11] measurements indicated that the G^-G^+ conformation (**G**$^-$**G**$^+$) coexists together with a TG conformer, with the energy difference between these two forms being ~0 kcal/mol.

For the first time, Wiberg and Murcko[6] applied ab initio molecular orbital computations to the DME problem and concluded that the "+sc,+sc" conformer (**G**$^-$**G**$^+$ or **G**$^+$**G**$^-$) was the ground-state conformer, followed by a "+sc,180°" conformer (**TG**$^-$). The energy difference was computed to be 1.22 kcal/mol at the MP2/6-31G* and 1.56 kcal/mol at the MP3/6-31G* between these two structures. Later Allinger et al.[12] also concluded that the gauche−gauche (**G**$^-$**G**$^+$) conformer of DME was the most stable, followed by an antigauche (**TG**$^-$) conformer, but by a smaller energy difference of 0.60 kcal/mol computed using MM3 method. However, Anderson et al.,[13] using the MM3(94) method, reported that a conformer other than an antigauche form was the second most populated conformer after the ground-state **G**$^-$**G**$^+$ conformer. Marcos et al.[14] identified three minima for gas-phase DME, with structures G^-g^- (**G**$^-$**G**$^+$), Tg^- (**TG**$^+$), and tt (**TT**), while a fourth minimum with a G^+g^- (**G**$^+$**G**$^+$) structure appeared only when solvent effects were taken into account.

The above discussion indicates that a closer look on the conformations of DME is certainly warranted. We have therefore, for the first time, studied the conformers of DME, using matrix isolation infrared spectroscopy. In these studies, we have employed both effusive and supersonic free jet expansion sources for depositing the matrix. We have also used a heated effusive source to deposit the matrix to increase the population of the higher-energy conformers and render them discernible in our experiments so that information on the higher-energy conformers can also be obtained. We have also performed ab initio computations on the structures, energies, and vibrational frequencies for the various conformers of DME, at the HF/6-31++G** and B3LYP/6-31++G** level, to corroborate our experimental results.

Experimental Section

Matrix isolation experiments were performed using a Leybold AG closed cycle helium compressor cooled cryostat, RD210. The details of the vacuum and cryogenic systems have been discussed elsewhere.[15−17]

DME (Fluka, >99%) and the matrix gas argon (IOLAR Grade I) were first mixed to the desired ratio (DME/Ar 1:1000) in a mixing chamber. This gas mixture was then deposited using an effusive source, onto a KBr substrate maintained at 12 K. The deposition rate was typically ~3 mmol h^{-1}, and typical deposition times lasted ~30 min. The deposition was performed at various effusive nozzle temperatures, ranging from 298 to 431 K. In the hot nozzle experiments, the nozzle was heated over a length of 35 mm to the required temperatures. Experiments were performed at elevated nozzle temperatures in an effort to observe spectral features corresponding to higher-energy conformers. At the maximum temperature of the nozzle (431 K), trace amounts of methanol were also observed following the reaction of DME with water,[18] which is an inevitable impurity in a vacuum systems. Experiments were also performed where the sample was deposited using a supersonic source. A pulsed molecular beam valve (Lasertechnics, Model LPV) was used to produce the supersonic beam.

The IR spectra (4000−400 cm^{-1}) of the deposited species were recorded using a Bomem MB 100 FTIR spectrometer with spectral resolution of 1 cm^{-1}. The matrix was then warmed to 35 K, kept at this temperature for about 30 min and then recooled to ~12 K. The spectra of the matrix thus annealed were again recorded.

Computational Methods

Ab initio molecular orbital calculations were performed using the Gaussian 94W program[19] on an Intel Pentium II 233 MHz machine. Geometry optimizations were done both at the HF and B3LYP level with analytical gradients, using a 6-31++G** basis set, to obtain minima corresponding to the various conformers. All geometric parameters were allowed to be optimized, and no constraints were imposed on the molecular geometry during the optimization process.

Vibrational frequencies were calculated both at the HF and B3LYP levels using a 6-31++G** basis set and analytical derivatives. The computed frequencies were then scaled to bring them in agreement with the experimental results. To arrive at the scaling factor, we chose the strongest feature in our experiment (i.e. 1143.6 cm^{-1} feature) that could be unambiguously assigned to the ground-state conformer and correlated it with that strongest computed feature for the ground-state conformer in this region. The factor that would bring this computed frequency in agreement with the experimental feature was then calculated and used to scale all other vibrational frequencies. It turned out that the scaling factor for the frequencies calculated at the HF/6-31++G** level was 0.8962 while that computed at the B3LYP/6-31++G** level was 0.9841. The B3LYP frequencies were used to compare our experimental frequencies with computations, as they provided a superior fit to our experimental data. Zero-point energies (ZPE) were also obtained from the frequency calculations, and the ZPEs after due scaling were used to calculate the ZPE-corrected relative energies for the different conformers.

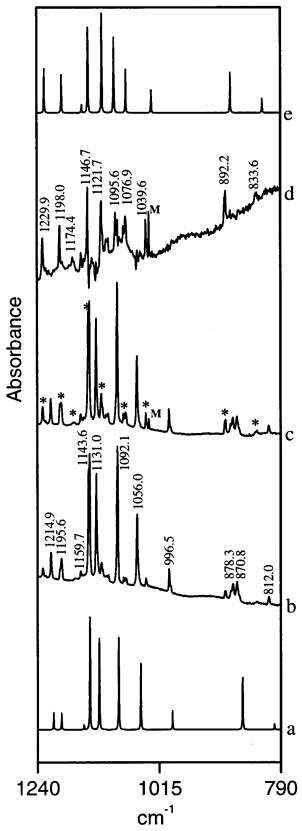

Figure 2. Computed and experimental spectra of DME. (a) Computed spectra for the ground-state $\mathbf{G^-G^+}$ conformer. Matrix-isolated FTIR spectra of DME/Ar (1:1000) using an effusive source where the nozzle temperature was maintained at (b) 298 and (c) 431 K. (d) Spectra obtained by subtracting spectra b from c. (e) Computed spectra for the $\mathbf{TG^-}$ conformer.

The computed frequencies of the various modes for the conformers of DME were then used to simulate the vibrational spectra. For this exercise, the frequencies and the relative intensities obtained at the B3LYP level were used and the spectra were then constructed assuming a Lorentzian line profile with a fwhm of 1 cm^{-1}, which is the typical line widths obtained in our experiments.

Results

Experimental Results. Figure 2 shows the infrared spectra of DME trapped in Ar in the region of 790−1240 cm^{-1}, which corresponds to the C−O stretching, CH_2 rocking, and CH_3 deformation vibrations. The DME/Ar ratio was 1:1000 in all these experiments. Figure 2b shows the spectrum of DME in a preannealed matrix; the deposition being done using an effusive nozzle maintained at room temperature. When the matrix was annealed at 35 K and the spectrum again recorded, no discernible changes in the spectral features were obtained.

We then deposited DME in Ar, using a supersonic free jet source. When a supersonic jet is used as a source to deposit the matrix, the population of the higher-energy conformers would be expected to be depleted in the cold beam. Consequently, the corresponding infrared features would decrease in intensity; as was observed in our studies on the conformations of trimethyl phosphate.[16,17] However, in the case of DME, the spectrum obtained with a supersonic source was again identical with that obtained using an effusive source; i.e., no peaks appeared to decrease in intensity in the matrix deposited using the supersonic jet compared with the effusive source. In later discussions, we will rationalize this observation.

TABLE 1: Structural Parameters[a] of the Five Conformers of DME Computed at the B3LYP/6-31++G Level**

parameter	G^-G^+	TG^-	TG^+	TT	G^+G^+
C^1-O^2	1.424	1.417	1.417	1.417	1.421
C^3-O^2	1.413	1.427	1.426	1.411	1.421
C^3-O^4	1.420	1.397	1.404	1.411	1.420
C^5-O^4	1.426	1.425	1.427	1.417	1.423
C^3-H^6	1.100	1.109	1.100	1.108	1.094
C^3-C^7	1.522	1.520	1.529	1.528	1.5300
C^5-H^8	1.098	1.095	1.098	1.101	1.097
C^5-H^9	1.092	1.092	1.092	1.092	1.092
C^5-H^{10}	1.096	1.101	1.095	1.100	1.097
C^1-H^{11}	1.100	1.100	1.100	1.100	1.097
C^1-H^{12}	1.096	1.101	1.101	1.101	1.099
C^1-H^{13}	1.092	1.092	1.092	1.092	1.092
C^7-H^{14}	1.093	1.094	1.095	1.095	1.093
C^7-H^{15}	1.093	1.093	1.093	1.094	1.093
C^7-H^{16}	1.094	1.094	1.094	1.095	1.095
$C^3-O^2-C^1$	114.2	114.9	114.9	114.7	117.5
$O^4-C^3-O^2$	112.2	108.4	108.7	104.5	112.2
$C^5-O^4-C^3$	116.2	114.6	116.7	114.8	119.9
$H^6-C^3-O^4$	102.8	109.9	104.0	109.2	104.5
$C^7-C^3-O^4$	114.2	107.6	113.7	111.4	114.8
$H^8-C^5-O^4$	111.7	111.3	112.0	111.4	112.1
$H^9-C^5-O^4$	106.1	106.4	105.7	106.5	105.6
$H^{10}-C^5-O^4$	111.6	110.9	111.3	112.5	113.0
$H^{11}-C^1-O^2$	110.9	112.3	112.3	112.5	111.4
$H^{12}-C^1-O^2$	111.6	111.5	111.3	111.4	112.6
$H^{13}-C^1-O^2$	106.6	106.7	106.8	106.5	106.1
$H^{14}-C^7-O^3$	109.5	110.7	110.2	111.1	108.3
$H^{15}-C^7-C^3$	111.2	109.2	111.2	109.0	113.1
$H^{16}-C^7-C^3$	110.0	110.2	110.1	111.0	110.4
$O^4C^3O^2C^1$	65.0	155.8	149.5	156.7	−56.4
$C^5\ O^4C^3O^2$	64.8	−64.7	59.8	205.1	101.6
$H^6C^3O^4O^2$	117.7	117.5	116.0	116.7	110.5
$C^7C^3O^4O^2$	−122.3	−121.3	−124.2	−120.7	−129.7
$H^6C^3O^2C^1$	−48.6	36.9	36.8	36.9	−168.0
$H^6C^3O^4C^5$	−177.4	52.9	175.8	−38.2	−147.9
$C^7C^3O^2C^1$	−168.8	−85.7	−84.7	−82.8	74.7
$C^7C^3O^4C^5$	−57.4	174.1	−64.4	84.5	−28.1
$H^8C^5O^4C^3$	73.1	64.7	68.1	57.3	65.8
$H^9C^5\ O^4H^8$	−241.6	−240.5	−241.8	−241.3	−242.0
$H^{10}C^5O^4H^8$	−122.6	−122.0	−123.1	−122.4	−123.6
$H^{11}C^1O^2C^3$	58.9	66.5	66.1	65.5	65.4
$H^{12}C^1O^2H^{11}$	−121.6	−122.2	−122.3	−122.4	−123.4
$H^{13}C^1O^2H^{11}$	118.7	118.9	119.0	118.9	118.2
$H^{14}C^7C^3O^2$	64.6	59.3	63.6	62.2	56.0
$H^{15}C^7C^3H^{14}$	−119.2	−120.0	−119.5	−120.2	−119.9
$H^{16}C^7C^3H^{14}$	119.6	120.2	119.2	119.8	118.6

[a] Bond lengths in angstroms and bond angles and dihedral angles in degrees.

Experiments were then performed using heated effusive nozzles, with the nozzle temperature maintained at 380 and 431 K. Figure 2c shows the spectrum obtained using the hot nozzle effusive source at 431 K. This spectrum again corresponds to a preannealed matrix. It can be seen that the intensity of certain features, marked with an asterisk, increased when compared with that obtained using a room-temperature effusive source (Figure 2b). The intensity of these features in fact progressive increased in intensity as the temperature of the nozzle was raised from 298 to 431 K. Hence, these features may be expected to arise due to the higher-energy conformers. It must also be noticed that spectra recorded at the higher nozzle temperatures also showed a feature due to the methanol (marked with an "M" in Figure 2c,d), as has already been indicated earlier.

We have also recorded spectra over the 1350 and 3000 cm^{-1} regions which correspond to the CH_3 deformation and C−H stretching vibrations. However, the features in these regions could not be clearly resolved for the two different conformations and hence are not shown nor discussed.

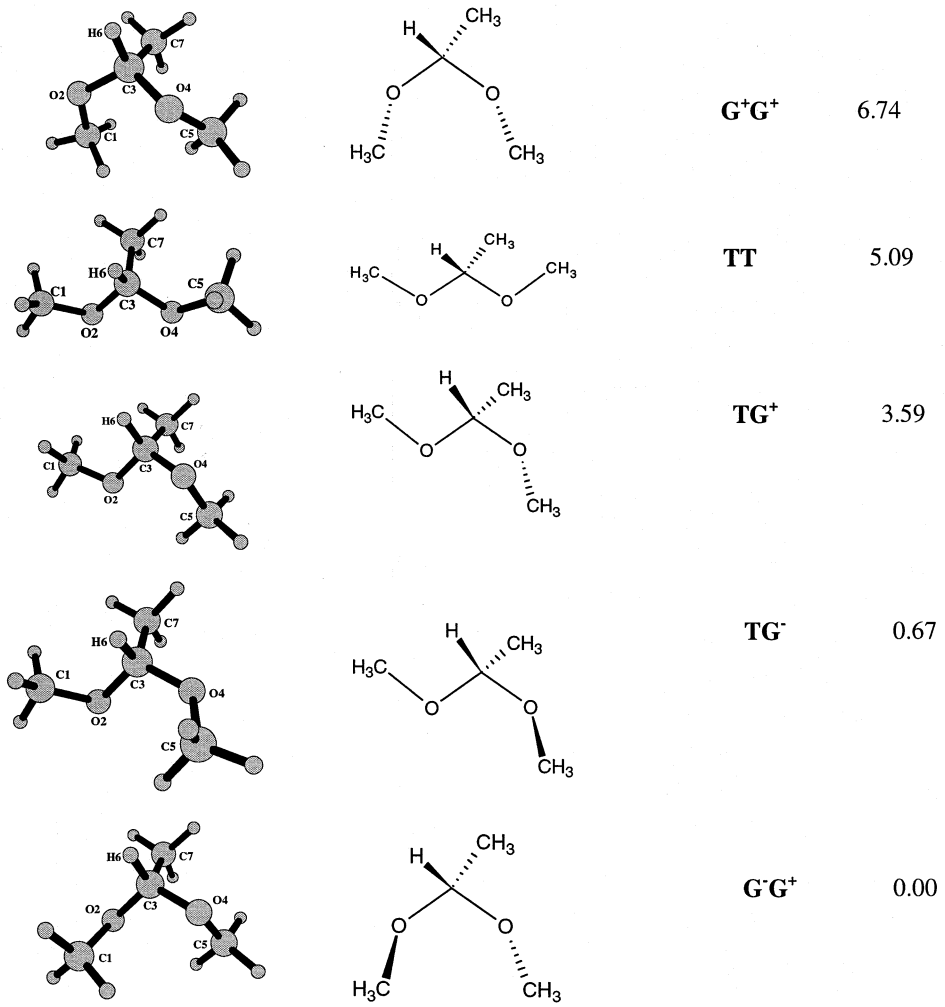

Figure 3. Conformations of DME corresponding to the five minima, $\mathbf{G^-G^+}$, $\mathbf{TG^-}$, $\mathbf{TG^+}$, **TT**, and $\mathbf{G^+G^+}$ calculated at the B3LYP/6-31++G**. The energy values mentioned against each structure are relative to the $\mathbf{G^-G^+}$ conformer, in kcal/mol.

All of the above experimental observations will now be discussed through a comparison with our computational results.

Computational Results. At the outset, we first performed geometry optimizations at the HF and B3LYP levels using a 6-31++G** basis set. In B3LYP level, we obtained five minima corresponding to conformations with $\mathbf{G^-G^+}$, $\mathbf{TG^-}$, $\mathbf{TG^+}$, **TT**, and $\mathbf{G^+G^+}$, structures, given in order of increasing energy. At the HF level, we obtained only four minima corresponding to $\mathbf{G^-G^+}$, $\mathbf{TG^-}$, **TT**, and $\mathbf{G^+G^+}$; at this level, the $\mathbf{TG^+}$ structure did not correspond to a minimum, as revealed by vibrational frequency calculations. The molecular parameters corresponding to the five minima obtained at the B3LYP/6-31++G** level are given in Table 1. The corresponding structures are shown in Figure 3. It must be noted that this the first report of the $\mathbf{TG^+}$ and $\mathbf{G^+G^+}$ minima for DME.

The relative energies of the conformers, corrected for zero-point energies, at the HF and B3LYP level obtained using a 6-31++G** basis are shown in Table 2. The calculated energy difference between $\mathbf{G^-G^+}$ and $\mathbf{TG^-}$ is 0.76 and 0.67 kcal/mol at the HF and B3LYP levels, respectively.

TABLE 2: Relative Energies[a] and Dipole Moments[b] of the Five Conformers of DME Calculated at the HF and B3LYP Levels Using a 6-31++G Basis Set**

	relative energy		dipole moment	
conformer	HF	B3LYP	HF	B3LYP
G^-G^+	0.00	0.00	0.23	0.22
TG^-	0.76	0.67	2.26	2.07
TG^+	–[c]	3.59	–[c]	1.62
TT	5.35	5.09	2.87	2.67
G^+G^+	7.53	6.74	2.57	2.49

[a] Energy relative to the $\mathbf{G^-G^+}$ conformer in kcal/mol. [b] Dipole moment in Debye. [c] $\mathbf{TG^+}$structure did not optimize to a minimum at the HF level.

Discussion

Vibrational Assignments. The spectral features at 812.0, 870.8, 878.3, 996.5, 1056.0, 1092.1, 1131.0, 1143.6, 1159.7, 1195.6, and 1214.9 cm^{-1}, marked in Figure 2b, are essentially those of the ground-state conformer, which is indicated from our computations to have a $\mathbf{G^-G^+}$ structure. The computed and scaled frequencies at the B3LYP level, for this conformer, agree well with the spectral features obtained with a room temperature effusive source, as can be seen from Table 3 and Figure 2, which shows the simulated features (Figure 2a) against the experimentally obtained spectrum (Figure 2b). However, there do appear certain features, marked with an asterisk in Figure 2c, that cannot be assigned to the ground-state $\mathbf{G^-G^+}$ conformer and probably belong to higher-energy conformers.

Our calculations, at the B3LYP/6-31G++**, indicates that the first higher-energy conformer with a $\mathbf{TG^-}$ structure lies about 0.67 kcal/mol above the ground-state conformer. The other higher-energy forms, $\mathbf{TG^+}$, **TT**, and $\mathbf{G^+G^+}$, lie 3.59, 5.09, and 6.74 kcal/mol respectively, above the ground state. At room

TABLE 3: Comparison of Experimental and B3LYP/6-31++G Computed Vibrational Frequencies in DME[a]**

conformer	B3LYP (unscaled)	B3LYP (scaled)[a]	experimental (MI)
G^-G^+	814.9	801.9 (7)[b]	812.0
	874.5	860.6 (71)	870.8, 878.3[c]
	1006.9	990.9 (23)	996.5
	1066.6	1049.6 (80)	1056.0
	1108.1	1090.5 (113)	1092.1
	1144.5	1126.3 (118)	1131.0
	1162.1	1143.6 (136)	1143.6
	1173.0	1154.3 (6)	1159.7
	1214.9	1195.6 (20)	1195.6
	1229.9	1210.3 (22)	1214.9
	1378.7	1356.8 (15)	1351.4, 1370.0, 1390.7, 2836.0, 2911.6, 2939.8, 2946.9, 2966.3, 2997.9, 3010.9[e]
	1400.0	1377.7 (8)	
	1422.1	1399.5 (42)	
	3004.4	2956.6 (54)	
	3018.2	2970.2 (105)	
	3022.4	2974.3 (13)	
	3058.3	3009.7 (10)	
	3076.6	3027.7 (38)	
	3083.6	3034.6 (47)	
	3133.5	3083.7 (32)	
	3135.9	3086.0 (10)	
	3138.3	3088.4 (22)	
	3138.5	3088.6 (25)	
TG^-	836.9	823.6 (17)	833.6
	896.7	882.4 (48)	892.2
	1045.5	1028.9 (28)	1039.6
	1093.1	1075.7 (53)	1076.9, 1080.6[c]
	1115.5	1097.8 (100)	1095.6
	1138.2	1120.1 (121)	1121.7
	1164.0	1145.5 (110)	1146.7
	1175.6	1156.9 (10)	1174.4
	1213.4	1194.1 (46)	1198.0
	1245.8	1226.0 (53)	1229.9
	1380.5	1358.6 (14)	1351.4, 1370.0, 1390.7, 2836.0, 2911.6, 2939.8, 2946.9, 2966.3, 2997.9, 3010.9[d]
	1392.9	1370.8 (31)	
	1420.9	1398.3 (54)	
	1488.2	1464.5 (11)	
	2912.2	2865.9 (68)	
	2987.9	2940.4 (69)	
	2999.9	2952.2 (71)	
	3039.4	2991.1 (55)	
	3055.1	3006.5 (19)	
	3087.5	3038.4 (40)	
	3128.5	3078.8 (30)	
	3131.3	3081.5 (19)	
	3140.5	3090.6 (18)	
	3142.7	3092.7 (24)	

[a] The computed intensities for each mode is given in parenthesis. [b] Scaling factor is 0.9841. [c] Computed intensities are in units of km/mole [d] The doublets may be due to site effects. [e] Features in the region 1300−3000 cm^{-1} have not been specifically assigned to either the $\mathbf{G^-G^+}$ or $\mathbf{TG^-}$ conformer.

temperature, the populations of each of the conformers (relative to the ground-state conformer) would be in the ratio $\mathbf{G^-G^+}$:$\mathbf{TG^-}$:$\mathbf{TG^+}$:$\mathbf{TT}$:$\mathbf{G^+G^+}$ = 100.0:32.3:0.2:0:0. It can be seen that the $\mathbf{TG^-}$ form contributes to almost ∼24% of the total population. It is therefore likely that the unassigned features in the spectrum shown in Figure 2b could be due to the $\mathbf{TG^-}$ form. If so, the intensities of these unassigned features should increase as the temperature of the effusive nozzle was increased.

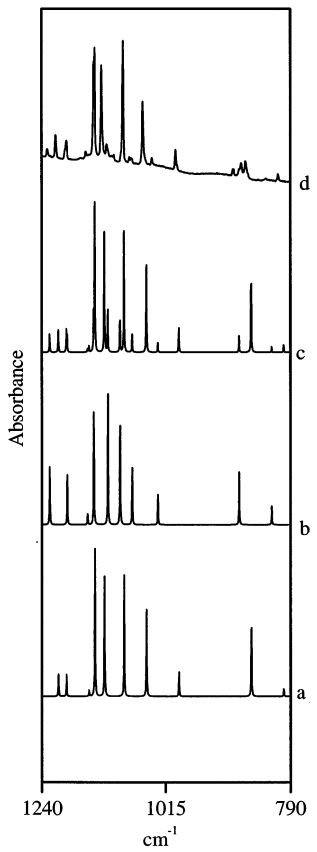

Figure 4. Comparison of synthetic and experimental spectra for DME. Computed spectra for conformers (a) $\mathbf{G^-G^+}$ and (b) $\mathbf{TG^-}$. (c) Sum of computed spectra for $\mathbf{G^-G^+}$ and $\mathbf{TG^-}$, weighted according to the populations of the two conformers at 298 K. (d) Matrix isolation spectra recorded using an effusive source at 298 K.

Figure 2c shows the spectrum obtained using a hot nozzle effusive source (nozzle temperature 431 K). It can be seen that the features that were left unassigned in Figure 2b increased in intensity in the hot nozzle experiments. At 431 K, the population of the $\mathbf{TG^-}$ conformer would increase to ∼31% from ∼24% at 298 K, while the populations of the $\mathbf{TG^+}$, $\mathbf{TT}$, and $\mathbf{G^+G^+}$ would still be insignificant (<1%). Consequently, the features that increased in intensity in the hot nozzle experiment can be attributed to the $\mathbf{TG^-}$ conformer. We subtracted the spectrum shown in Figure 2c (431 K nozzle) from that shown in Figure 2b (298 K nozzle), and the subtracted spectrum is shown in Figure 2d. Figure 2e shows the computed spectrum of the $\mathbf{TG^-}$ conformer, where the frequencies and intensities were obtained from the B3LYP computations and the simulation was done using a Lorentian line profile and a fwhm of 1 cm^{-1}. It can be seen that spectra in Figure 2d,e agree well, confirming that the subtracted spectrum shown in Figure 2d does indeed correspond to the $\mathbf{TG^-}$ form, which constitutes the first reported infrared spectrum of the $\mathbf{TG^-}$ conformer of DME. Table 3 gives the computed and experimental frequencies for both the $\mathbf{G^-G^+}$ and $\mathbf{TG^-}$ conformers. The overall error in the fit of the computed frequencies to experiment is 8.0 cm^{-1}.

In Figure 4, we compare the experimental matrix isolation spectra obtained using an effusive source at 298 K, with a computed synthetic spectra obtained by adding the computed spectra for conformers $\mathbf{G^-G^+}$ and $\mathbf{TG^-}$ weighted according to their relative populations at 298 K. It can be seen that there is an excellent agreement between the two spectra.

It must be noted that in comparing the experimental frequencies with our computations, only the B3LYP computations were

considered. As described in our work on DMM,[7] the HF frequencies did not provide a good fit of the computed frequencies with our experiments and hence were not considered.

In contrast to the observations in DME where the spectral features of the higher-energy **TG**$^-$ conformers were clearly discernible even in the room-temperature spectra, in the case of DMM,[7] the higher-energy **TG**$^\pm$ conformer become observable only at elevated temperatures or concentrations. This observation is supported by our computations, which indicate a larger energy difference between the ground and first higher-energy conformers in DMM (2.30 kcal/mol) than those in DME (0.67 kcal/mol).

The normal mode descriptions in the acetals are quite complex because of the coupling of various C−O stretching and C−H deformation modes. Dasgupta et al.[20] have pointed out that contributions from the two types of force constants are almost about equal and the dominant character of any of the vibrations cannot be unambiguously assigned. We therefore made no attempt in this work to make a detailed assignment of the various frequencies.

Dipole Moments. Goodman et al.[8] reported the dipole moment of DME in benzene to be 1.65 D at 298 K. The computed dipole moments of the various DME conformers using both HF/6-31++G** and B3LYP/6-31++G** are shown in Table 2. It can be seen that the computed dipole moment values at the HF and B3LYP levels were not very different at the two levels of calculations. Using the computed dipole moments at the B3LYP level for each conformer, the dipole moment of DME averaged over the different conformers was calculated. In this calculation, the **TG**$^+$, **TT** and **G**$^+$**G**$^+$ conformers were assumed not to contribute to the overall dipole moment of DME as these conformers, with energies >3.5 kcal/mol, would not be expected to contribute significantly to the overall conformational population at room temperature. The dipole moment of DME thus calculated is 1.04 D at 298 K, which can be compared with the experimental value Goodman et al. of 1.65 D. It must be noted that the experimental dipole moment of DME (1.65 D) is larger than that of DMM (0.67 D). If it is recalled that the dipole moment of the **TG** conformer is greater than the **G**$^-$**G**$^+$ conformers in both DMM and DME, this would indicate that the **TG** conformer contributes more significantly in DME than in DMM, in agreement with our calculations and matrix isolation experiments.

Barrier to Conformer Interconversion. When DME was trapped in an argon matrix using an effusive source and the matrix then annealed at 35 K, the spectral features due to the **TG**$^-$ conformer did not disappear, indicating that the barrier for interconversion is greater than of 10 kJ/mol (2.4 kcal/mol).[21] Similarly, no changes in the spectral features were observed in the supersonic cooling experiments as compared with the effusive sampling. This observation again indicates that cooling in the free jet expansion is not sufficient to surmount the barrier from **TG**$^-$ to **G**$^-$**G**$^+$. In our earlier work on DMM and trimethyl phosphate (TMP), supersonic cooling did significantly deplete the population of the higher-energy conformers, thus indicating that the barrier to conformer interconversion in DME is likely higher than in the other two molecules.

Comparison of the Conformational Picture in DMM and DME. The substitution of a methyl group for one of the hydrogens on the central carbon atom of DMM leads to a lowering of symmetry in DME. A diagram (Figure 5) can therefore be drawn to correlate the conformations of the two molecules. The ground state for both molecules has the **G**$^-$**G**$^+$ (or the degenerate **G**$^+$**G**$^-$) orientation. The stability of this conformer is decided by the operation of two anomeric interactions involving the nonbonded electrons of both the oxygens. At the B3LYP/6-31++G** level, the energy difference between **G**$^-$**G**$^+$ and the first excited **TG**$^-$ conformer in DME (0.67 kcal/mol) was smaller than that in DMM (2.30 kcal/mol). This observation indicates that the relative importance of the **G**$^-$**G**$^+$ conformer in DME was decreased as compared with that in DMM. This is due to the unfavorable steric interaction of the methyl group on the central carbon atom (C3) with the terminal methyl group gauche to it (C5).

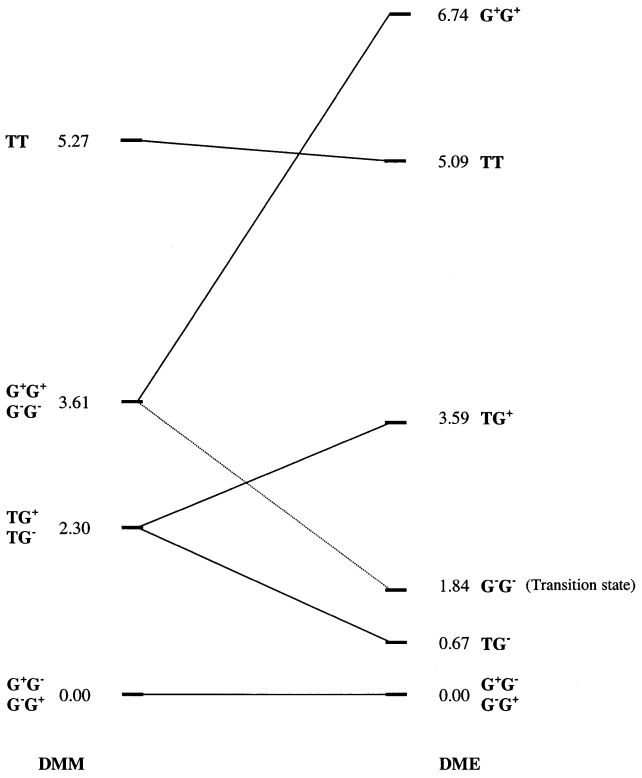

Figure 5. Diagram showing the correlation between the conformers in DMM and DME.

The first higher-energy conformer for DMM is a **TG** structure; the symmetry of the molecule precludes discrimination of the two degenerate **TG**$^+$ and **TG**$^-$ forms. The TG structure in DME, however, splits into **TG**$^-$ and **TG**$^+$, with the **TG**$^-$ structure lower in energy than the **TG**$^+$ form. In the **TG**$^-$ conformer, the anomeric interaction involving the electrons on one of the oxygens is suppressed, causing this conformer to be higher in energy than the ground-state **G**$^-$**G**$^+$. In addition to the splitting of the degeneracy, the **TG** structures in DMM and DME show further differences. In DMM, one of the terminal methyl group is oriented in a near-perfect trans orientation ($O^4C^3O^2C^1$ dihedral is ∼180°), while in DME the same dihedral angle is ∼155°. This slight distortion is caused by the steric interaction of the C3 methyl with the C1 methyl. The C5 methyl is gauche oriented with almost the same angles in both molecules ($C^5O^4C^3O^2$ dihedral ∼65°), thus effecting an anomeric interaction. In the **TG**$^-$ conformer in DME, the C5 methyl is oriented away from the C3 methyl, while in the **TG**$^+$ conformer, it is oriented on the same side, but with the same dihedral angles in both cases. Understandably, the steric interactions in the **TG**$^+$ conformer is more enhanced compared with that in the **TG**$^-$ conformer, making the **TG**$^-$ lower in energy relative to the **TG**$^+$.

A third structure in DMM is the **G**$^\pm$**G**$^\pm$ form. In this structure, both the terminal methyl groups (C1 and C5) are oriented on

the same side, and their mutual interaction causes this conformer to be placed in energy above the $\mathbf{G}^-\mathbf{G}^+$ and $\mathbf{TG}^\pm$ forms. In DME, this corresponding structure splits into $\mathbf{G}^-\mathbf{G}^-$ and $\mathbf{G}^+\mathbf{G}^+$. In the first conformer, the two terminal methyl groups are oriented away from the C3 methyl, while in the latter, they are on the same side. Our computations showed that the $\mathbf{G}^-\mathbf{G}^-$ structure turns out to be a saddle point (with one imaginary frequency), while the $\mathbf{G}^+\mathbf{G}^+$ structure corresponds to a minimum, but with the highest energy among all the conformers of DME. This structure enjoys the anomeric interaction involving the electrons on both the oxygens; however, the steric interactions pushes this conformer to the top of the energy list. The **TT** structure in DME, where no anomeric interactions exist, turns out to be lower in energy than the $\mathbf{G}^+\mathbf{G}^+$ form. Incidentally, an IRC calculation showed that the $\mathbf{G}^-\mathbf{G}^-$ saddle point connects the $\mathbf{G}^-\mathbf{G}^+$ and $\mathbf{TG}^-$ forms.

An analysis of the structural parameters reveals the relative interplay of anomeric and steric interactions in determining the relative stabilities of the different conformers. As in DMM,[7] the variation of the C3−O2 and C3−O4 bond lengths in the different conformers of DME presents clear signatures of the $n-\sigma^*_{CO}$ anomeric interaction (delocalization of the oxygen lone pair into a low lying anti adjacent σ^*_{c-o} orbital). It can be seen from Table 1 that the C3−O2 and C3−O4 bond lengths in the $\mathbf{G}^-\mathbf{G}^+$ conformer are longer than the corresponding bonds in the **TT** conformer. The lengthening of the two C−O bonds in the $\mathbf{G}^-\mathbf{G}^+$ conformer relative to the **TT** structure is due to the anomeric interaction, which is present in the gauche (G) orientation only. Likewise, the C3−O2 bond length is longer than the C3−O4 bond in the $\mathbf{TG}^-$ and $\mathbf{TG}^+$ structures, as the anomeric interaction is present only in that part of the molecule with the gauche orientation.

We also examined the possibility if any intramolecular hydrogen bonding interactions were involved in stabilizing any of these conformers. An examination of the charge density topology using the atoms-in-molecule (AIM) theory of Bader[22] showed no (3,−1) bond critical points in DME that could be associated with intramolecular C−H...O interactions. It must therefore be concluded that anomeric and steric effects are the major contributing factors for conformer stability in DME. In 1,2-dimethoxyethane, however, Matsuura had proposed the existence of intramolecular C−H...O interactions,[23] which, in fact, was corroborated by our AIM analysis for that molecule.

Conclusions

We have trapped both $\mathbf{G}^-\mathbf{G}^+$ and $\mathbf{TG}^-$ conformers in an argon matrix using effusive as well as supersonic source and recorded its infrared spectra for the first time. The experimental vibrational frequencies for both the conformers agreed well with the calculated frequencies at the B3LYP level. This work has led to definitive assignment of the various infrared features of DME observed in the matrix isolation spectra. A thorough search of the potential has also been conducted to arrive at other possible higher-energy conformers of DME and new minima were identified corresponding to the $\mathbf{TG}^+$ and $\mathbf{G}^+\mathbf{G}^+$ conformers.

Acknowledgment. V.V. gratefully acknowledges the grant of a research fellowship from the Department of Atomic Energy, India.

References and Notes

(1) Juraisti, E.; Cuevas, G. *The Anomeric Effect*; CRC Inc: London, 1995.
(2) Deslongchamps, P. *Stereoelectronic Effects in Organic Chemistry*; Pergamon: Oxford, 1983.
(3) Thatcher, G. R. J. *The Anomeric Effect and Associated Stereoelectronic Effects*; American Chemical Society: Washington, DC, 1993.
(4) Kneisler, J. R.; Allinger, N. L. *J. Comput. Chem.* **1996,** *17*, 757.
(5) Smith, G. D.; Jaffe, R. L.; Yoon, D. Y. *J. Phys. Chem.* **1994**, *98*, 9072.
(6) Wiberg, K. B.; Murcko, M. A. *J. Am. Chem. Soc.* **1989**, *111*, 4821.
(7) Venkatesan, V.; Sundararajan, K.; Sankaran, K.; Viswanathan, K. S. *Spectrochim. Acta* **2002**, *58A*, 467.
(8) Goodman, M.; Niu, G. C. C. *Macromolecules* **1968**, *1*, 223.
(9) Saur, O.; Janin, A.; Vallet, A.; Lavalley, J. C. *J. Mol. Struct*. **1976**, *34*, 171.
(10) Kintzinger, J. P.; Delseth, C.; Nguyên, T. T. T. *Tetrahedron* **1980**, *36*, 3431.
(11) Abe, A.; Inomata, K.; Tanisawa, E.; Ando, I. *J. Mol. Struct*. **1990**, *238*, 315.
(12) Allinger, N. L.; Rahman, M.; Lii, J. H. *J. Am. Chem. Soc.* **1990**, *112*, 2, 8293.
(13) (a) Anderson, J. E.; Heki, K.; Hirota, M.; Jørgensen, F. S. *J. Chem. Soc., Chem. Commun.* **1987**, 554. (b) Anderson, J. E. *J. Org. Chem.* **2000**, *65*, 748.
(14) Marcos, E. S.; Pappalardo, R. P.; Chiara, J. L.; Domene, M. C.; Martinez, J. M.; Parrondo, R. M. *J. Mol. Struct. (THEOCHEM)* **1996**, *371*, 245.
(15) George, L.; Sankaran, K.; Viswanathan, K. S.; Mathews, C. K. *Appl. Spectrosc.* **1994**, *48*, 7.
(16) Vidya, V.; Sankaran, K.; Viswanathan, K. S. *Chem. Phys. Lett.* **1996**, *258*, 113.
(17) George, L.; Viswanathan, K. S.; Singh, S. *J. Phys. Chem. A* **1997**, *101*, 2459.
(18) Chen, J.; Fritz, J. S. *Anal. Chem.* **1991**, *63*, 2016.
(19) Frisch, M. J.; Trucks, G. W.; Schlegel, H. B.; Gill, P. M. W.; Johnson, B. G.; Robb, M. A.; Cheeseman, J. R.; Keith, T.; Petersson, G. A.; Montgomery, J. A.; Raghavachari, K.; Al-Laham, M. A.; Zakrzewski, V. G.; Ortiz, J. V.; Foresman, J. B.; Peng, C. Y.; Ayala, P. Y.; Chen, W.; Wong, M. W.; Andres, J. L.; Replogle, E. S.; Gomperts, R.; Martin, R. L.; Fox, D. J.; Binkley, J. S.; Defrees, D. J.; Baker, J.;. Stewart, J. J. P.; Head-Gordon, M.; Gonzalez, C.; Pople, J. A. *Gaussian 94*, Revision B.3; Gaussian, Inc.: Pittsburgh, PA, 1995.
(20) Dasgupta, S.; Smith, K. A.; Goddard, W. A., III. *J. Phys. Chem*. **1993**, *97*, 10891.
(21) Barnes, A. J. In *Matrix Isolation Spectroscopy*; Barnes, A. J., Orville-Thomas, W. J., Müller, A., Gaufrès, R., Eds.; Reidel Publishing Co.: Dordrecht, The Netherlands, 1981; Chapter 23.
(22) Bader, R. F. W. *Atoms in Molecules*; Calendon Press: Oxford, 1994.
(23) Yoshida, H.; Kaneko, I.; Matsuura, H.; Ogawa, Y.; Tasumi, M. *Chem. Phys. Lett*. **1992**, *196*, 601.